



# A Paradigm Shift in Nuclear Chromatin Interpretation: From Qualitative Intuitive Recognition to Quantitative Texture Analysis of Breast Cancer Cell Nuclei

Hye-Kyung Lee,<sup>1\*</sup> Cho-Hee Kim,<sup>2</sup> Subrata Bhattacharjee,<sup>3</sup> Hyeon-Gyun Park,<sup>3</sup>   
 Deekshitha Prakash,<sup>3</sup> Heung-Kook Choi<sup>3\*</sup>

<sup>1</sup>Department of Pathology, College of Medicine, Eulji University, Daejeon, Korea

<sup>2</sup>Department of Digital Anti-Aging Healthcare, u-AHRC, Inje University, Gimhae, Korea

<sup>3</sup>Department of Computer Engineering, u-AHRC, Inje University, Gimhae, Korea

Received 7 April 2020; Revised 2 October 2020; Accepted 2 November 2020

Grant sponsor: Ministry of Trade, Industry and Energy, Grant number P0002072

Additional Supporting Information may be found in the online version of this article.

\*Correspondence to: Prof. Heung-Kook Choi, Department of Computer Engineering, Inje University, Republic of Korea. Email: cschk@inje.ac.kr Prof. Hye-Kyung Lee, Department of Pathology, Eulji University Medical College, Republic of Korea. Email: hlee@eulji.ac.kr

Published online 15 November 2020 in Wiley Online Library (wileyonlinelibrary.com)

DOI: 10.1002/cyto.a.24260

© 2021 The Authors. *Cytometry Part A* published by Wiley Periodicals LLC on behalf of International Society for Advancement of Cytometry.

This is an open access article under the terms of the Creative Commons Attribution-NonCommercial License, which permits use, distribution and reproduction in any medium, provided the original work is properly cited and is not used for commercial purposes.

## • Abstract

Assessing the pattern of nuclear chromatin is essential for pathological investigations. However, the interpretation of nuclear pattern is subjective. In this study, we performed the texture analysis of nuclear chromatin in breast cancer samples to determine the nuclear pleomorphism score thereof. We used three different algorithms for extracting high-level texture features: the gray-level co-occurrence matrix (GLCM), gray-level run length matrix (GLRLM), and gray-level size zone matrix (GLSZM). Using these algorithms, 12 GLCM, 11 GLRLM, and 16 GLSZM features were extracted from three scores of breast carcinoma (Scores 1–3). Classification accuracy was assessed using the support vector machine (SVM) and k-nearest neighbor (KNN) classification models. Three features of GLCM, 11 of GLRLM, and 12 of GLSZM were consistent across the three nuclear pleomorphism scores of breast cancer. Comparing Scores 1 and 3, the GLSZM feature *large zone high gray-level emphasis* showed the largest difference among breast cancer nuclear scores among all features of the three algorithms. The SVM and KNN classifiers showed favorable results for all three algorithms. A multiclass classification was performed to compare and distinguish between the scores of breast cancer. Texture features of nuclear chromatin can provide useful information for nuclear scoring. However, further validation of the correlations of histopathologic features, and standardization of the texture analysis process, are required to achieve better classification results. © 2021 The Authors. *Cytometry Part A* published by Wiley Periodicals LLC on behalf of International Society for Advancement of Cytometry.

## • Key terms

nuclear chromatin; texture analysis; breast carcinoma; classification; histopathologic; pattern

**EVALUATION** of the nuclear chromatin pattern is essential for pathological investigations (1). Nuclear chromatin provides important genetic and biological information; the chromatin pattern serves as a visual symbol of hidden biological processes (2). The chromatin pattern can be described as hyperchromatic, hypochromatic, coarse granular, fine granular, vesicular, or “salt and pepper,” and so on. Each chromatin pattern can be sufficiently unique that it can serve as a useful marker for tumor diagnosis. However, the chromatin structure is ambiguously defined, which has motivated efforts toward developing objective tools, such as image analysis methods. Texture image analysis constitutes an objective, quantitative assessment based on their gray levels and their spatial relationship in an image (3,4). The most widely used texture analysis methods are the co-occurrence and run-length matrices (5). A gray-level co-occurrence matrix (GLCM) shows how often various combinations of pixel brightness values occur in an image. Each element of  $p(i, j)$  specifies the number of times a pixel with a gray-level value,  $i$ , occurs, shifted by a given



distance to a pixel with a value  $j$ . In a gray-level run length matrix (GLRLM), the pixel  $p(i, j)$  is defined as the number of runs with pixels of gray level,  $i$ , and run-length,  $j$  (6-8). In a coarse texture, relatively long gray-level runs occur, while a fine texture will show short runs. The recently introduced gray-level size zone matrix (GLSZM) represents two-dimensional data based on GLRLM. GLSZM detects pixels that are identical to a reference pixel in the periphery, stores the number of connected pixels in the matrix, and calculates feature values based on these stored values (9,10). In the field of histopathology, several studies have been conducted using GLCM and GLRLM, but studies using GLSZM are rare. Breast cancer is one of the most common cancer in women and the nuclear grade has major clinical implications and Nottingham histologic score is widely used for determining the nuclear grade of breast cancer based on three factors: tubule formation, nuclear pleomorphism, and the mitotic cell count (11). Among three factors, nuclear pleomorphism is the most subjective element of the histological grade (12). Given that nuclear pleomorphism is mainly determined by chromatin texture, we performed a texture analysis of nuclear chromatin in breast carcinoma samples using GLCM, GLRLM, and GLSZM, and the results were compared with the score of nuclear polymorphism. Thus, we can assess the potential for a paradigm shift from qualitative intuitive perception to quantitative texture analysis of nuclear chromatin interpretation.

## MATERIALS AND METHODS

### Tissue Samples

We analyzed three surgically resected invasive ductal carcinomas with nuclear pleomorphism score of 1 (SC-1), 2 (SC-2), and 3 (SC-3), which were diagnosed by independent two pathologists who were blinded to the original diagnosis. This study was performed according to the Helsinki Declaration and was approved by the Ethics Committee of Eulji University Hospital (IRB No: 2019-10-016). All formalin-fixed paraffin-embedded tissues were sectioned with a thickness of 4  $\mu\text{m}$  and stained with hematoxylin and eosin compounds according to the standard method using an autostainer. Our image analysis technique consisted of five phases, as shown in Figure 1: image acquisition using a digital camera; breast cancer cell nuclei segmentation; extraction of texture features using GLCM, GLRLM, and GLSZM; statistical analysis; and breast cancer grading using the support vector machine (SVM) and k-nearest neighbor (KNN) algorithms.

### Image Acquisition

Breast cancer tissue images of each nuclear pleomorphism score were acquired by a pathologist using a digital camera at 600 $\times$  magnification (DP73; Olympus, Tokyo, Japan) attached to a microscope (BX-51; Olympus) under the same condition. Neoplastic cells were acquired in 14 bits/pixel color bitmap format (2.01 megapixels per image). The image resolution was 4,800  $\times$  3,800 pixels. The image sensor size was 1/1.8 in. and the pixel size was 4.40  $\times$  4.40  $\mu\text{m}$ . We collected a total of

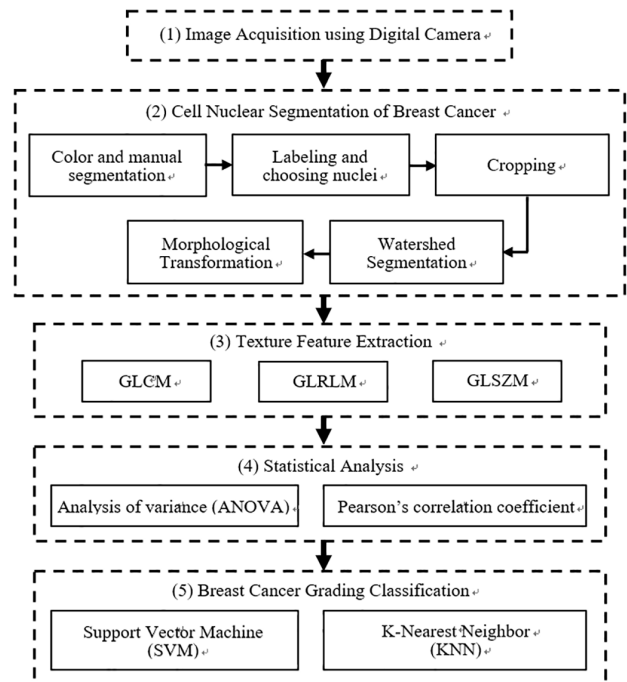


**Figure 1.** Overview of the proposed pipeline for texture analysis and nuclear scoring of breast carcinoma. GLCM: gray-level co-occurrence matrix, GLRLM: gray-level run length matrix, GLSZM: gray-level size zone matrix.

31 images (eight images of SC-1, 12 of SC-2, and 11 of SC-3) from three breast cancer patients. Examples of histopathological images of each nuclear pleomorphism score of breast carcinoma are shown in the Supporting Information, Appendix SI, and Figure S1a–c. Each of the following scores is assigned according to the Nottingham histologic scoring system as follows:

SC-1: Small, regular, uniform nuclei.

SC-2: Moderate increase in size and variability.

SC-3: Marked variation.

### Nuclear Segmentation of Cancer Cells

The SC-1 and SC-2 nuclear images were converted from red, green, blue (RGB) color space to  $L^*a^*b^*$  color space. Color segmentation was performed based on various threshold values, shown in Figure 2a–c. For SC-3 images, manual segmentation was performed due to poor results after automatic color segmentation. After segmentation, a pathologist (H.K. L.) reviewed thoroughly the segmented images and compared them with the original ones obtained from HE stain. Non-neoplastic cells such as vascular endothelia or stromal cells were discarded by the pathologist. Also, the objects smaller than 150 pixels were removed automatically, shown in Figure 2d,e, and then we labeled the nuclei for overlapping segmentation and sent it to the pathologist for nucleus selection. The nuclei in Figure 3b were selected by a pathologist and the overlapping nuclei were stored in a separate image for watershed segmentation. After cropping the connected cell

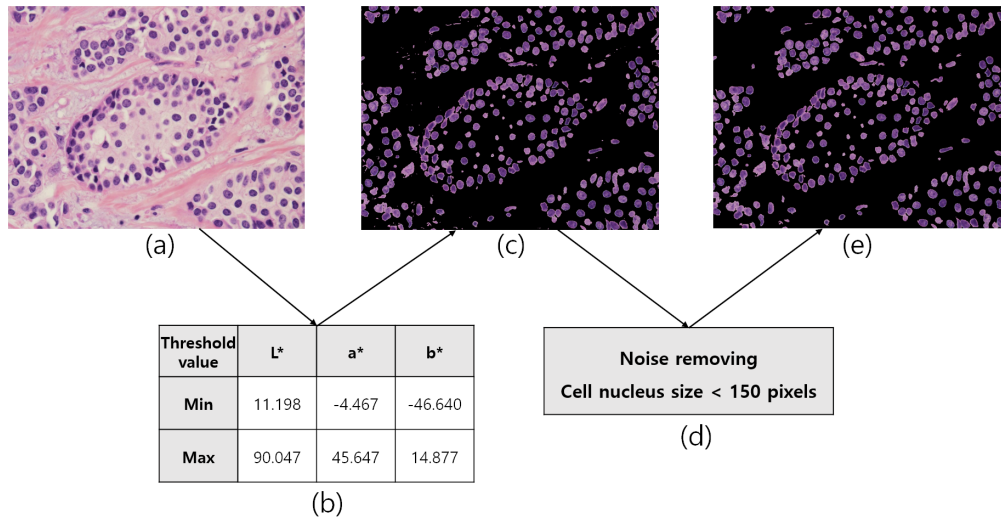


**Figure 2.** Nuclear segmentation. (a) Original image. (b) Minimum and maximum threshold values for color separation. (c) L\*a\*b\* color segmentation. (d) A threshold value for removing noisy pixels. (e) De-noised image extracted from (c). [Color figure can be viewed at [wileyonlinelibrary.com](http://wileyonlinelibrary.com)]

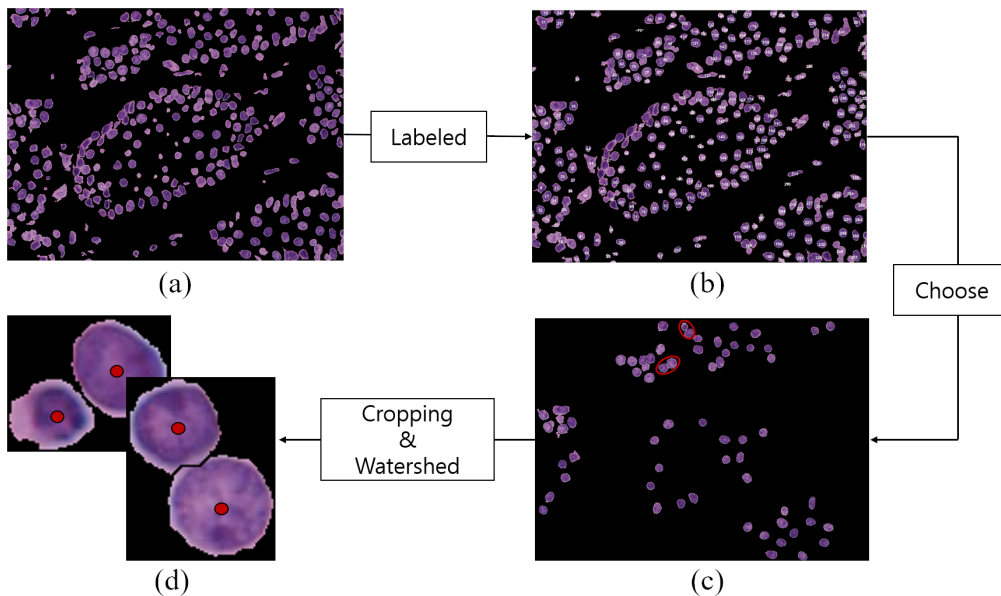


**Figure 3.** Overlapping nuclei segmentation using a watershed algorithm. (a) Pre-processed image after L\*a\*b\* color segmentation. (b) Labeled image. (c) Nuclei selection is based on a pathologist’s decision. (d) Result of watershed segmentation. The red dot in (c) indicates the overlapping nuclei and the red dots in (d) are the markers. [Color figure can be viewed at [wileyonlinelibrary.com](http://wileyonlinelibrary.com)]

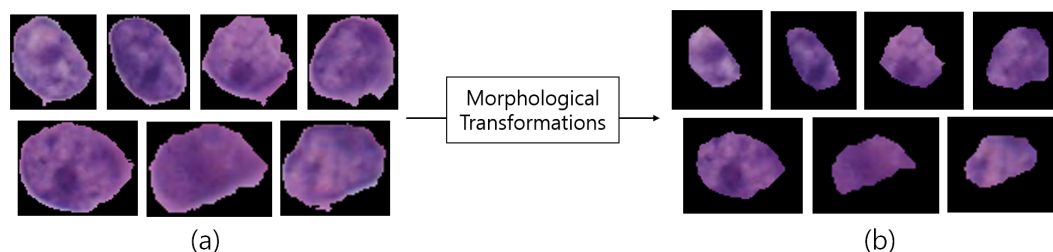
nucleus, the color image was converted to binary format, and the distance transform algorithm was applied to calculate the distance map (13). Finally, markers were placed on each nucleus based on the distance map, and a watershed algorithm was performed to separate the overlapping nuclei for texture analysis, shown in Figure 3d.

Figure 4 shows the morphological transformations of segmented nuclei. Three morphological operations (erosion, opening, and closing) were applied to remove peripheral brightness and smooth the nuclear membrane boundary. For the SC-1 and SC-2 samples, all three morphological

operations were applied to trim the nuclear shape and extract chromatin texture information from the cell nucleus; however, for the SC-3 sample, erosion was not applied because of the previous manual segmentation.

**Texture Feature Extraction**

Texture analysis provides information about the spatial patterns of intensity and color and is typically performed using statistical-, moment-, spectral energy-, and form-based methods (14). We carried out statistical-based techniques, namely GLCM, GLRLM, and GLSZM. Statistical texture



**Figure 4.** Morphological transformations of segmented nuclei. (a) Cropped images after watershed segmentation. (b) Nuclear contour smoothing using morphological operations, namely erosion, opening, and closing. Finally, we obtained a total of 1,320 nuclear images (440 nuclei for each SC-1, SC-2, and SC-3, respectively). [Color figure can be viewed at [wileyonlinelibrary.com](http://wileyonlinelibrary.com)]

analysis describes the relationship among pixels in the image according to their gray-level values, where GLCM and GLRLM are typical algorithms used for this purpose. GLCM can describe the inter-pixel relationships and GLRLM describes the relationships in linear one-dimensional terms; GLSZM is an extended version of GLRLM that describes the gray-level size zone in two dimensions.

A list of abbreviations for all the textural features extracted in this study is provided in the Supporting Information Appendix SI and Abbreviation. Conversion from RGB to gray-level was performed as follows:  $R \times 0.2989 + G \times 0.587 + B \times 0.114$ . The matrices were created using grayscale levels in the range of 0–255. The pixel navigation angles were 0, 45, 90, and 135°, and the mean result was calculated for all four directions.

### Gray-Level Co-Occurrence Matrix

GLCM, which describes second-order statistical texture properties and provides the informations regarding the positions of pixels having similar gray-level values, was proposed by Haralick et al. (5). After determining the displacement vector,  $d = (dx, dy)$ , of the matrix, the intensity values are used to calculate the frequency of occurrence of pairs of pixels separated by  $d$  and to generate a matrix describing the spatial distribution of intensity (15). The matrix is normalized as the sum of each element divided by the total number of pairs of pixels. Characteristic values that can be calculated using the normalized GLCM include angular second moment, inverse differential moment, entropy, correlation, contrast, homogeneity, correlation, and diagnostic moment values (16). The basic principle of GLCM is shown in the Supporting Information Appendix SI and Figure S2. In this article, a two-dimensional,  $256 \times 256$  GLCM was constructed with grayscale levels in the range of 0–255, based on the four directions 0°, 45°, 90°, and 135° at a distance of  $d = 1$ . During GLCM computation, pixels with a zero value were not considered in the matrix. The extracted 12 features of GLCM were energy, entropy, correlation, contrast, homogeneity, variance, sum mean, inertia, cluster shade, cluster tendency, maximum probability, and inverse variance; the formulae used to calculate these features and their characteristics are given in the Supporting Information Appendix SI and Table S1.

### Gray-Level Run Length Matrix

GLRLM, which analyses statistical texture by calculating the length of homogeneous runs for each gray level, was introduced by Galloway (6). The matrix describes the gray intensity pattern of pixels in a specific direction relative to reference pixels; run length is the range of adjacent pixels with the same gray intensity in that direction. The basic principle of GLRLM is shown in the Supporting Information Appendix SI and Figure S3. The extracted 11 features of GLRLM were short-run emphasis (SRE), long-run emphasis (LRE), gray-level non-uniformity (GLNU), run length non-uniformity (RLN), run percentage (RP), low gray-level run emphasis (LGRE), high gray-level run emphasis (HGRE), short-run low gray-level emphasis (SRLGE), short-run high gray-level emphasis (SRHGE), long-run low gray-level emphasis (LRLGE), and long-run high gray-level emphasis (LRHGE); the formulae used to calculate these 11 features are given in Supporting Information Appendix SI and Table S2.

### Gray-Level Size Zone Matrix

GLSZM was introduced by Thibault (9,10) and is based on the size of a pixel zone that is different from GLCM and GLRLM. No specific direction is used when calculating GLSZM features. The number of neighboring pixels around a reference pixel having the same gray level is counted and stored in a matrix. The resulting matrix is determined by the size of the largest zone. The 8-connectivity was used for assessing neighboring pixels in this study, as with the example shown in the Supporting Information Appendix SI and Figure S4. The extracted 16 texture features of GLSZM calculated in this article were small zone emphasis (SZE), large zone emphasis (LZE), low gray-level zone emphasis (LGLZE), high gray-level zone emphasis (HGLZE), small zone low gray-level emphasis (SZLGLE), small zone high gray-level emphasis (SZHGLE), large zone low gray-level emphasis (LZLGLE), large zone high gray-level emphasis (LZHGLE), GLNU, normalized gray-level non-uniformity (NGLNU), zone size non-uniformity (ZSNU), normalized zone size non-uniformity (NZSNU), zone percentage (ZP), gray-level variance (GLV), zone size variance (ZSV), and zone size entropy (ZSE); the formulae used to calculate these features and their description are given in Supporting Information Appendix SI and Table S3.

### Statistical Analysis

Two tests were used to analyze statistically whether the extracted texture features have a significant impact on the nuclear pleomorphism scoring of breast carcinoma. First, one-way analysis of variance (ANOVA), a method of hypothesis testing that uses *F*-values created by comparing the variances within and between the groups, was performed (17). Here, distribution analysis was used to determine whether there was a difference in mean values among scores. Texture features with an *F*-value of less than 5 or a *P*-value greater than 0.05 were excluded, as was GLCM cluster shade ( $P > 0.05$ ). Second, we performed Pearson's correlation coefficient. High correlation coefficients were indicated by a linear tendency. As shown in the Supporting Information Appendix SI and Figure S5, the two distributions of SZE with significantly different correlation coefficients. From among the total of 39, we selected 24 texture features for classification testing based on their *F*-values, *p*-values, and strong correlations ( $r > 0.9$ ). To analyze the magnitude differences between the nuclear pleomorphism scores and feature importance, the effect size (Cohen's *f* and eta squared) has been computed using *F*-values, numerator degrees of freedom, and denominator degrees of freedom obtained from the ANOVA hypothesis test, shown in the Appendix SI and Table S4.

### Classification Model

After preprocessing and feature calculation, classification was performed based on two machine-learning algorithms: support vector machine (SVM) and *k*-nearest neighbor (KNN). Supervised learning techniques were used in this study: for training, labeled data samples were used to determine the discriminant function, while various newly labeled data samples were used to test the derived function. Fivefold cross-validation was used to validate the training set. During our classification based on the texture characteristics of cell nuclei in histological sections of breast carcinomas, both SVM and KNN performed well.

SVM is typically used for binary classification; the algorithm searches for the optimal boundaries for discriminating and classifying data (18), shown in the Supporting Information Appendix SI and Figure S6. Six classifiers were used to carry out SVM classification in this study, namely linear, quadratic, cubic, fine Gaussian, medium Gaussian, and coarse Gaussian.

KNN is an important method that does not require any assumptions to be met regarding the distribution of the data. This simple classification algorithm uses the minimum distance from the query instance to the training samples to determine the class that the majority of the "*k*" nearest neighbors belong to (19). Six classifiers were used to carry out KNN classification in this study, namely fine, medium, coarse, cosine, cubic, and weighted KNN. This algorithm stores all available cases and classifies new cases based on similarity measures, as shown in the Supporting Information Appendix SI and Figure S7. The KNN classifier is a nonparametric method used for classification and regression.

### RESULTS AND DISCUSSION

A data set of texture features based on GLCM, GLRLM, and GLSZM was created for each nuclear pleomorphism score. Chromatin texture data were extracted from a total of 1,320 nuclear images (440 nuclei for each SC-1, SC-2, and SC-3). The data set was divided into training and testing data sets according to an 8:2 ratio. The mean and standard deviation values for the size of the nuclei are as follows:  $708 \pm 220 \mu\text{m}^2$  for SC-1,  $871 \pm 220 \mu\text{m}^2$  for SC-2, and  $2,275 \pm 928 \mu\text{m}^2$  for SC-3. We hypothesized that when the nuclear score is determined by the degree of nuclear atypia and the texture features, the mean values of these features will tend to increase or decrease consistently with nuclear score due to the continuous nuclear scoring system spectrum.

For the selection of meaningful features according to nuclear score, we focused on: (1) the consistency of textural features; (2) the difference between SC-1 and SC-3; and (3) data reduction after statistical analysis. In the view of consistency, all of the GLRLM and GLSZM features showed a consistent trend, except for the following four GLSZM features: LZLGLE, NGLNU, ZSNU, and GLV. However, only three GLCM features were consistent: contrast, inertia, and inverse variance. Figure 5 shows example graphs of consistent and inconsistent GLCM and GLSZM features.

In the view of between SC-1 and SC-3, Figure 6 shows the feature value ratios, which represent feature difference, derived by dividing the mean feature values of SC-1 by those of SC-3 (colored in blue). If the result of SC-3 was more than SC-1, its reciprocal (SC-3/SC-1) was calculated instead (colored in red). Among the three different texture analysis methods, no feature for GLCM had a ratio exceeding the arbitrary value of 2, shown in Figure 6a.

Figure 6b,c shows the results GLRLM and GLSZM, respectively. The GLRLM features with the highest two mean SC-1/SC-3 values were SRLGE and SRE, and those with the highest two mean SC-3/SC-1 values were LRHGE and GLNU. The GLSZM features with the highest two mean SC-1/SC-3 values were SZLGE and LGLE, and those with the highest two mean SC-3/SC-1 values were LZHGLE and ZSV. Among the three different texture analysis methods, the GLSZM feature LZHGLE showed the largest difference between SC-1 and SC-3.

In the view of data reduction after statistical analysis, 24 features were selected from among all 39, based on their strong correlations ( $r > 0.9$ ) and high *F*-values. These were included 6 GLCM features (entropy, contrast, variance, sum mean, max probability, and inverse variance), 6 GLRLM features (LRE, RLN, RP, HGRE, SRLGE, and LRHGE), and 12 GLSZM features (SZE, HGLZE, SZLGLE, LZLGLE, LZHGLE, GLNU, NGLNU, ZSNU, NZSNU, ZP, GLV, and ZSE). Regarding the nuclear pleomorphism score of breast cancer, chromatin texture-based classification using KNN and SVM showed accuracies of 83.7% and 84.1% for GLCM, 93.9% and 91.7% for GLRLM, 93.2% and 93.6% for GLSZM, and 94.3% and 93.9% for the combined (GLCM, GLRLM, and GLSZM) features, respectively. Table 1 shows the overall

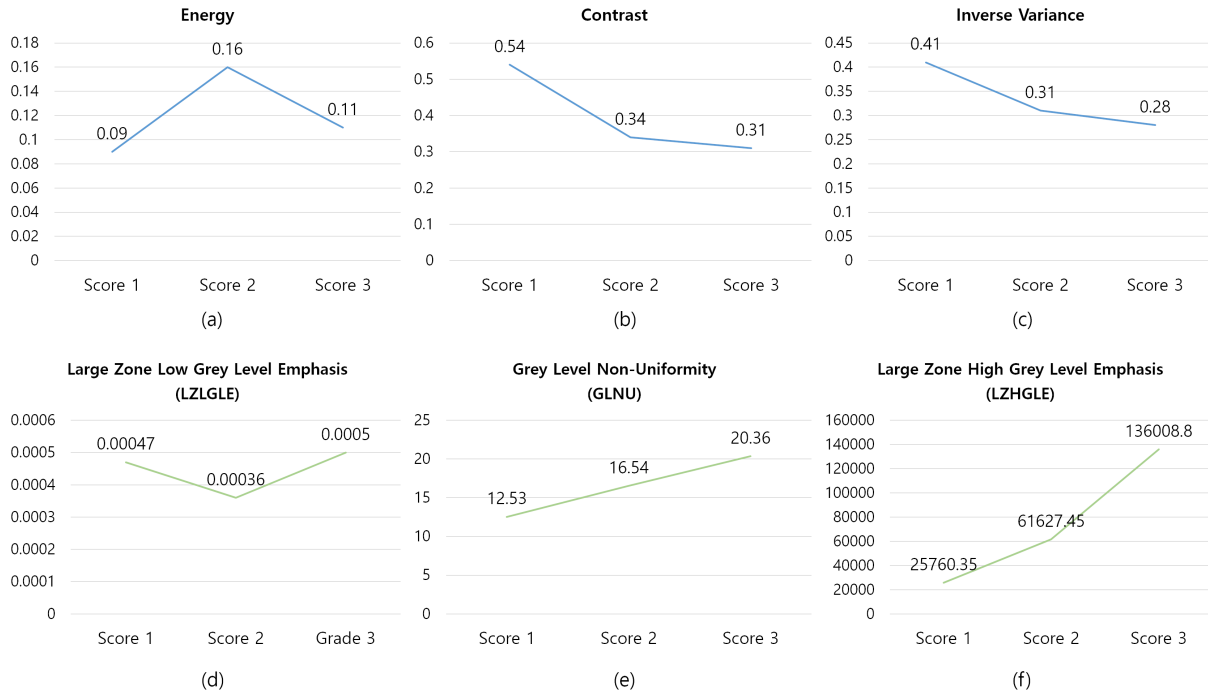


**Figure 5.** Example graphs of consistent and inconsistent features in the gray-level co-occurrence matrix (GLCM) and gray-level size zone matrix (GLSZM). (a,d) Inconsistent values can be seen for the GLCM feature of energy and the GLSZM feature of LZLGLE, respectively. (b,c,e,f) Consistent values can be seen for the GLCM features of contrast and inverse variance, and the GLSZM features of GLNU and LZHGLE, respectively. [Color figure can be viewed at wileyonlinelibrary.com]

classification results of breast carcinoma, and the performance of the classifier has been evaluated using four types of metrics namely, accuracy, precision, recall, and f1-score. Among these, recall is the most important metric, which indicates the accurate classification for each score.

From the obtained results, we have analyzed that GLCM features significantly affected the performance of the classifiers and achieved the lowest accuracy, whereas the features of GLRLM and GLSZM afforded high accuracy and can be considered as highly accurate features for classifying SC-1, SC-2, and SC-3. Combinations that include GLCM, GLRLM, and GLSZM features had the highest accuracy compared to other classification groups. The confusion matrices in the Supporting Information Appendix SI and Tables S5-S8 were obtained from the machine learning classification.

Considering that the three factors of consistency along the scores, difference ratio > 2 between SC-1 and SC-3, and statistical analysis are important for the selection of meaningful features from the three matrices; four features of GLRLM (LRE, RP, SRLGE, and LRHGE) and four features of GLSZM (HGLZE, SZLGLE, LZHGLE, GLV) were selected.

However, mathematical review of the functions of the features revealed the similarity of the functions, such as GLRLM's SRLGE  $\left( \left( \frac{1}{N_r(\theta)} \right) \sum_{i=1}^{N_g} \sum_{j=1}^{N_r} \frac{P(i,j|\theta)}{i^2 j^2} \right)$  and GLSZM's SZLGLE  $\left( \left( \frac{1}{N_z} \right) \sum_{i=1}^{N_g} \sum_{j=1}^{N_r} \frac{P(i,j)}{i^2 j^2} \right)$ , GLRLM's LRHGE  $\left( \left( \frac{1}{N_r(\theta)} \right) \sum_{i=1}^{N_g} \sum_{j=1}^{N_r} i^2 j^2 P(i,j|\theta) \right)$

and GLSZM's LZHGLE  $\left( \left( \frac{1}{N_z} \right) \sum_{i=1}^{N_g} \sum_{j=1}^{N_r} i^2 j^2 P(i,j) \right)$  which was understandable based on the fact that GLSZM is an extended version of GLRLM (9,10).

And also, it was interesting to note that the two of the selected four features of GLRLM (LRE and SRLGE) are related to the low gray level, and the two of the selected four features of GLSZM (HGLZE and LZHGLE) are related to the high gray level, which suggests the likelihood of that low gray level is more detectable to the line-based GLRLM, and the high gray level is more detectable to size-based GLSZM.

In terms of statistical analysis and data reduction, of the hundreds of potential features, the choice of key texture feature is important. For instance, the similar accuracy of all 39 of the features included in this study, and among the 24 selected features, highlights the importance of selecting statistically significant features. The similar accuracy and strong correlations of the features can be understood in terms of the similarity in the mathematical functions of each feature.

In the view of comparison and integration of histologic findings with texture analysis, our result was supportive. As mentioned in the Supporting Information Appendix SI and Tables S1-S3, the histologic findings of fine, regular chromatin can be translated into short, small, and repetitive features while hypo- and hyperchromatism can be translated into high and low gray-level features in GLCM, GLRLM, and GLSZM,

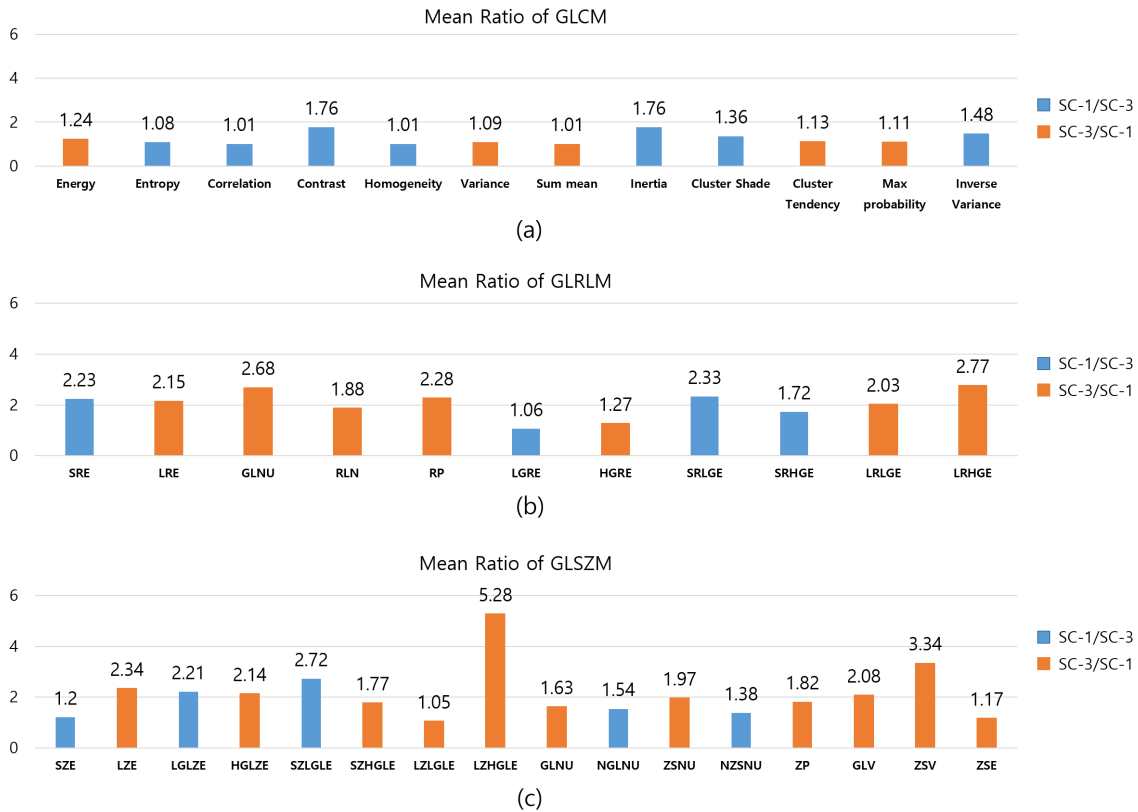


**Figure 6.** Feature difference analysis of SC-1/SC-3 and SC-3/SC-1. (a) GLCM, (b) GLRLM, and (c) GLSZM. (See the main text for the feature abbreviations for GLRLM and GLSZM shown in [b] and [c], respectively.) [Color figure can be viewed at wileyonlinelibrary.com]

**Table 1.** The overall classification performance was obtained from the test data set of GLCM, GLRLM, and GLSZM

CLASSIFIER	ACCURACY	PRECISION	RECALL	F1-SCORE
<b>GLCM</b>				
K nearest neighbor	83.7	83.7	83.6	83.6
Support vector machine	84.1	83.0	84.0	83.5
<b>GLRLM</b>				
K nearest neighbor	93.9	94.0	93.8	93.8
Support vector machine	91.7	91.6	91.6	91.6
<b>GLSZM</b>				
K nearest neighbor	93.2	93.2	93.2	93.2
Support vector machine	93.6	93.5	93.5	93.5
<b>Combination of GLCM, GLRLM, and GLSZM</b>				
K nearest neighbor	94.3	94.4	94.3	94.3
Support vector machine	93.9	93.9	93.9	93.9

respectively. In results, SC-1 nuclei with regular fine chromatin pattern showed higher mean values for the SRE, SRLGE, and SRHGE of GLRLM, and SZLGLE of GLSZM while SC-3 nuclei with irregularly coarse granular hyper and hypochromatic chromatin pattern showed higher mean values for the LRHGE feature in GLRLM and LZHGLE feature in GLSZM (Fig. 5). However, Given that the pattern of irregular, hyperchromatic, vesicular, coarse granular chromatin is the

nuclear pattern of pleomorphic SC-3 cells, in contrast to the low difference ratio of LZLGLE suggesting large hyperchromatin in SC-3, the large difference ratio of LZHGLE suggesting large hypochromatin in SC-3 may be related to the likelihood that high grayscale levels will have a greater impact than low grayscale levels. And this finding seems to be related to a tendency to be more susceptible to a high gray level in GLSZM than GLRLM, as we mentioned.

The features of each algorithm in this study showed specificity for each nuclear pleomorphism score. Given the high accuracy of the GLSZM features for SC-3, in contrast to the high accuracy of the GLCM features for SC-1, it seems to be important to select the appropriate algorithm based on the nuclear chromatin pattern. GLCM would be more appropriate for describing periodic textures such as fine, granular carcinoid tumors, endocrine lesions, or low-grade nuclei (e.g., SC-1 nuclei), whereas GLSZM would be more appropriate for describing more regional, heterogeneous, and non-periodic textures, such as pleomorphic or high-grade tumors, or high-grade nuclei (e.g., SC-3 nuclei). Considering our daily use of two-dimensional glass slides, the parameters of the two-dimensional GLSZM are closer to our intuitive interpretation than GLCM or GLRLM.

Mathematical approaches for analyzing tissue cross sections have been applied since the late 1970s (20, 21) and image analysis tools have sparked renewed interest in such approaches.

Each GLCM, GLRLM, and GLSZM feature function is defined as a combination of squares, divisions, and integrals using the constants composed mainly of gray intensity and spatial relationship of pixels such as run lengths, size zones. The features represent the microscopic findings of granularity, coarseness, and chromatism of the nuclei. However, similar functions with different constants of each matrix such as GLRLM's SRLGE and GLSZM's SZLGE or GLRLM's LRHGE and GLSZM's LZHGLE warn of a high correlation between them.

Despite the high accuracy, the lack of generalization of our results to common invasive ductal carcinoma still remains due to arbitrary difference ratio  $> 2$ , the limited number of tumors and samples, as well as the biological and histological heterogeneity within or between tumors. However, we hope that the experiments integrating the qualitative perception of histological findings and the features of quantitative texture analysis could be meaningful in the field of histopathology. Recalling that GLSZM has been introduced as the expansion matrix of GLRLM and that a new matrix such as neighborhood gray tone difference matrix has recently been developed, our anticipated open mind for a new matrix is essential.

In image processing in other medical fields, such as radiology, texture analysis studies (the so-called radiomics) have been performed for assessing image heterogeneity (22). However, texture analysis has been performed less frequently in the field of histology (23-27). With the features of GLCM, GLRLM, and GLSZM, histologic findings regarding the regularity, granularity, hypochromatism, and hyperchromatism of chromatin texture can be analyzed, and higher diagnostic power can thus be achieved based on such objective and reproducible data.

## CONCLUSION

Image analysis based on texture parameters is difficult, while that based on length and size (i.e., morphometric measurements) is relatively simple. However, overcoming the difficulties with texture-based analysis in the field of diagnostic

cytopathology is important, especially to reduce the subjective individual interpretation of nuclear chromatin patterns. Our study aimed to determine whether the texture features of nuclear chromatin can provide useful information for nuclear grading. Using 12 texture features of GLCM, 11 of GLRLM, and 16 of GLSZM, a total of 1,320 segmented nuclei images of breast cancer (440 nuclei each for SC-1, SC-2, and SC-3) were studied in terms of their ability to facilitate nuclear scoring. Considering the consistency along the scores, and difference ratio  $> 2$  between SC-1 and SC-3, four features of GLRLM (LRE, RP, SRLGE, and LRHGE) and four features of GLSZM (HGLZE, SZLGE, LZHGLE, GLV) were significant with the largest difference in LZHGLE of GLSZM. The LZHGLE of GLSZM is meaningful in the view of textural image expression of the histologic finding of large hypochromatic nuclei of high grade cancer.

High concordance with nuclear pleomorphism score and classification accuracy rates exceeding 90% were achieved using SVM and KNN, suggesting that texture parameters can indeed provide useful information on nuclear chromatin patterns.

However, many challenges remain. First, the selection of key texture features from among the hundreds of potential features now available due to developments in mathematics is important. For instance, the similar accuracy of all 39 of the features included in this study, and among the 24 selected features, highlights the importance of selecting statistically significant features. The similar accuracy and strong correlations of the features can be understood in terms of the similarity in the mathematical functions of each feature. Although we selected the 24 features based on Pearson's correlation and ANOVA, to identify ideal features from among many similar ones, more comprehensive mathematical manipulations, and validation of the correlations of histopathologic features, will be needed. Second, reliable nuclear segmentation is both necessary and challenging; particularly for high-grade nuclei, this is a fundamental problem. At the outset, we planned to perform automatic nuclear segmentation in our study, but ultimately we had to apply manual segmentation to SC-3 nuclei because of the high failure rate of automatic segmentation. Considering the significant impact of segmentation on the final results, standardization of image resolution and more effective segmentation are required. Comprehensive research on standardization and validation of variables, mathematical manipulations of different matrices, and the integration of histologic findings and texture analysis will help us overcome the challenges.

## ACKNOWLEDGMENT

This research was financially supported by the Ministry of Trade, Industry, and Energy (MOTIE), Korea, under the "Regional Specialized Industry Development Program (R&D, P0002072)" supervised by the Korea Institute for Advancement of Technology (KIAT).

## AUTHOR CONTRIBUTIONS

**Hyekyung Lee:** Investigation; resources; validation; writing-original draft. **Chohee Kim:** Formal analysis; methodology. **Subrata Bhattacharjee:** Formal analysis; investigation; methodology; visualization; writing-review and editing. **Hyeonyun Park:** Formal analysis; methodology; software. **Deekshitha Prakash:** Formal analysis; writing-review and editing. **H. K. Choi:** Funding acquisition; supervision; visualization.

## CONFLICT OF INTEREST

The authors have no conflict of interest to declare.

## LITERATURE CITED

- Zink D, Fischer AH, Nickerson JA. Nuclear structure in cancer cells. *Nat Rev Cancer* 2004;4:677–687.
- He S, Dunn KL, Espino PS, Drohic B, Li L, Yu J, Sun JM, Chen HY, Pritchard S, Davie JR. Chromatin organization and nuclear microenvironments in cancer cells. *J Cell Biochem* 2008;104:2004–2015.
- Gurcan MN, Boucheron LE, Can A, Madabhushi A, Rajpoot NM, Yener B. Histopathological image analysis: A review. *IEEE Rev Biomed Eng* 2009;2:147–171.
- Bhattacharjee S, Mukherjee J, Nag S, Marita I, Bandyopadhyay SK. Review on histopathological slide analysis using digital microscopy. *Int J Adv Sci Technol* 2014;62:65–96.
- Haralick RM, Shanmugam K, Dinstein I. Textural features for image classification. *IEEE Trans Syst Man Cybern* 1973;3:610–621.
- Galloway MM. Texture analysis using gray level run lengths. *Comput Graph Image Process* 1975;4:172–179.
- Chu A, Sehgal CM, Greenleaf JF. Use of gray value distribution of run lengths for texture analysis. *Pattern Recogn Lett* 1990;11:415–419.
- Tang X. Texture information in run-length matrices. *IEEE Trans Image Process* 1998;7:1602–1609.
- Thibault G, Angulo J, Meyer F. Advanced statistical matrices for texture characterization: Application to cell classification. *IEEE Trans Biomed Eng* 2014;61:630–637.
- Thibault G, Fertil B, Navarro C, Pereira S, Cau P, Levy N, Sequeira J, Mari J-L. Texture indexes and gray level size zone matrix: Application to cell nuclei classification. 10th international conference on pattern recognition and information processing. 2009; 140–145.
- Santos M, Correia C, Marcos R, Santos A, Matos A, Lopes C, Pereira P. Value of the Nottingham histological grading parameters and Nottingham prognostic index in canine mammary carcinoma. *Anticancer Res* 2015;35:4219–4277.
- Dunne B, Going JJ. Scoring nuclear pleomorphism in breast cancer. *Histopathology* 2001;39:259–265.
- Bhattacharjee S, Park HG, Kim CH, Prakash D, Madusanka N, So JH, Choi HK. Quantitative analysis of benign and malignant tumors in histopathology: Predicting prostate cancer grading using SVM. *Appl Sci* 2019;9:1–17.
- Häberle L, Wagner F, Fasching PA, Jud SM, Heusinger K, Loehberg CR, Hein A, Bayer CM, Hack CC, Lux MP, et al. Characterizing mammographic images by using generic texture features. *Breast Cancer Res* 2012;14:1–12.
- Lee BI, Choi HJ, Choi HK. The study about imaging technique of texture features. *Proc Spring Conf Korea Multimed Soc* 2001;6:169–172.
- Pathak B, Barooah D. Texture analysis based on the gray-level co-occurrence matrix considering possible orientations. *Int J Adv Res in Electr, Electron Instrum Eng* 2013;2:4206–4212.
- Kim CH, So JH, Park HG, Madusanka N, Prakash D, Bhattacharjee S, Choi HK. Analysis of texture features and classifications for the accurate diagnosis of prostate cancer. *Korea MultiMed Soc* 2019;22:832–843.
- Bouazza SH, Hamdi N, Zeroual A, Auhmani K. Gene-expression-based cancer classification through feature selection with KNN and SVM classifiers. *Intell Syst Compute Vision* 2015;2015:1–6.
- Kim J, Kim BS, Savarese S. Comparing image classification methods: K-nearest neighbor and support-vector-machines. *Proceeding of WSEAS International Conference on Computer Engineering and Applications*. 2012; 133–138.
- Prewitt JM. Graphs and grammars for histology: An introduction. *Proc Annu Symp Comput Appl Med Care* 1979;17:18–25.
- Preston K Jr. Tissue section analysis: Feature selection and image processing. *Pattern Recognit* 1981;13:17–36.
- Lubner MG, Smith AD, Sandrasegaran K, Sahani DV, Pickhardt PJ. CT texture analysis: Definitions, applications, biologic correlates, and challenges. *Radiographics* 2017;37:1483–1503.
- Filipczuk P, Fevens T, Krzyżak A, Obuchowicz A. GLCM and GLRLM based texture features for computer-aided breast cancer diagnosis. *J Med Inform Technol* 2012;19:109–115.
- Wei L, Gan Q, Ji T. Cervical cancer histology image identification method based on texture and lesion area features. *Comput Assist Surg* 2017;22:186–199.
- Saito A, Numata Y, Hamada T, Horisawa T, Cosatto E, Graf HP, Kuroda M, Yamamoto Y. A novel method for morphological pleomorphism and heterogeneity quantitative measurement: Named cell feature level co-occurrence matrix. *J Pathol Inform* 2016;7:36.
- Jørgensen AS, Rasmussen AM, Andersen NKM, Andersen SK, Emborg J, Røge R, Østergaard LR. Using cell nuclei features to detect colon cancer tissue in hematoxylin and eosin stained slides. *Cytom Part A* 2017;91A:785–793.
- Zhang L, Kong H, Ting Chin C, Liu S, Fan X, Wang T, Chen S. Automation-assisted cervical cancer screening in manual liquid-based cytology with hematoxylin and eosin staining. *Cytom Part A* 2014;85A:214–230.